GigaScience

Artifact-free whole-slide imaging with structured illumination microscopy and Bayesian image reconstruction
--Manuscript Draft--

Manuscript Number:	GIGA-D-19-00306R2	
Full Title:	Artifact-free whole-slide imaging with structured illumination microscopy and Bayesian image reconstruction	
Article Type:	Data Note	
Funding Information:	National Institute of General Medical Sciences (1R15GM128166-01)	Dr Guy M Hagen
	Division of Biological Infrastructure (1727033)	Dr Guy M Hagen

Abstract:	Background Structured illumination microscopy (SIM) is a method which can be used to image biological samples and can achieve both optical sectioning and super-resolution effects. Optimization of the imaging setup and data processing methods results in high quality images without artifacts due to mosaicking or due to the use of SIM methods. Reconstruction methods based on Bayesian estimation can be used to produce images with a resolution beyond that dictated by the optical system. Findings Five complete datasets are presented including large panoramic SIM images of human tissues in pathophysiological conditions. Cancers of the prostate, skin, ovary, and breast, as well as tuberculosis of the lung, were imaged using SIM. The samples are available commercially and are standard histological preparations stained with hematoxylin and eosin. Conclusion The use of fluorescence microscopy is increasing in histopathology. There is a need for methods which reduce artifacts when employing image stitching methods or optical sectioning methods such as SIM. Stitched SIM images produce results which may be useful for intraoperative histology. Releasing high quality, full slide images and related data will aid researchers in furthering the field of fluorescent histopathology.

Corresponding Author:	Guy M Hagen, PHD UNITED STATES
Corresponding Author Secondary Information:	
Corresponding Author's Institution:	
Corresponding Author's Secondary Institution:	
First Author:	Karl A Johnson
First Author Secondary Information:	
Order of Authors:	Karl A Johnson
	Guy M Hagen, PHD
Order of Authors Secondary Information:	

Response to Reviewers:	Dear Editor: We would like to re-submit our manuscript entitled "Artifact-free whole-slide imaging with structured illumination microscopy and Bayesian image reconstruction" for

<table>
<tr><td></td><td>consideration in GigaScience as a data note. We made the following revisions.</td></tr>
</table>

consideration in GigaScience as a data note. We made the following revisions.

1. The reviewer noticed that two of the data files was incomplete or corrupted. We reloaded these two files.

2. We included a table showing the organization of the data files along with their sizes.

3. We included a universal public domain dedication text file with the dataset.

4. We added a statement about ethics approval and consent to participate.

5. We moved all of the information from the supplement into the main paper. We removed the example of the cellular-scale imaging.

Please note that the figures in the automatically generated PDF look terrible as usual. Two of the figures look like blank black boxes. There is nothing I can do about this. Please click the links embedded in the PDF to view the figures.

We hope that our paper will now be acceptable for publication in GigaScience.

Sincerely,

Guy M. Hagen

Additional Information:

Question	Response
Are you submitting this manuscript to a special series or article collection?	No
Experimental design and statistics Full details of the experimental design and statistical methods used should be given in the Methods section, as detailed in our Minimum Standards Reporting Checklist. Information essential to interpreting the data presented should be made available in the figure legends. Have you included all the information requested in your manuscript?	Yes
Resources A description of all resources used, including antibodies, cell lines, animals and software tools, with enough information to allow them to be uniquely identified, should be included in the Methods section. Authors are strongly encouraged to cite Research Resource Identifiers (RRIDs) for antibodies, model organisms and tools, where possible.	Yes

Have you included the information requested as detailed in our [Minimum Standards Reporting Checklist](#)?	
Availability of data and materials All datasets and code on which the conclusions of the paper rely must be either included in your submission or deposited in [publicly available repositories](#) (where available and ethically appropriate), referencing such data using a unique identifier in the references and in the "Availability of Data and Materials" section of your manuscript. Have you have met the above requirement as detailed in our [Minimum Standards Reporting Checklist](#)?	Yes

1   **Artifact-free whole-slide imaging with structured illumination microscopy**

2   **and Bayesian image reconstruction**

3   **Karl A Johnson[1], Guy M. Hagen[1*]**

4   *[1]UCCS center for the Biofrontiers Institute, University of Colorado at Colorado Springs*

5   *1420 Austin Bluffs Parkway, Colorado Springs, Colorado, 80918, USA*

6   *ghagen@uccs.edu

7   Guy Hagen: 0000-0002-4802-9481

8   **Abstract**

9   **Background** Structured illumination microscopy (SIM) is a method which can be used to image biological

10   samples and can achieve both optical sectioning and super-resolution effects. Optimization of the imaging

11   setup and data processing methods results in high quality images without artifacts due to mosaicking or due

12   to the use of SIM methods. Reconstruction methods based on Bayesian estimation can be used to produce

13   images with a resolution beyond that dictated by the optical system.

14   **Findings** Five complete datasets are presented including large panoramic SIM images of human tissues in

15   pathophysiological conditions. Cancers of the prostate, skin, ovary, and breast, as well as tuberculosis of the

16   lung, were imaged using SIM. The samples are available commercially and are standard histological

17   preparations stained with hematoxylin and eosin.

18   **Conclusion** The use of fluorescence microscopy is increasing in histopathology. There is a need for methods

19   which reduce artifacts when employing image stitching methods or optical sectioning methods such as SIM.

20   Stitched SIM images produce results which may be useful for intraoperative histology. Releasing high quality,

21   full slide images and related data will aid researchers in furthering the field of fluorescent histopathology.

22   **Keywords** Structured illumination microscopy, SIM, image stitching, Bayesian methods, MAP-SIM,

23   SIMToolbox, histopathology, cancer.

24   **Data description**

25   **Context**

26   Structured illumination microscopy (SIM) is a method in optical fluorescence microscopy which can

27   achieve both optical sectioning (OS-SIM) [1] and resolution beyond the diffraction limit (SR-SIM) [2,3]. SIM has

28   been used for super-resolution imaging of both fixed and live cells [4–7] and has matured enough as a method that it

29   is now available commercially. In SIM, a set of images is acquired using an illumination pattern which shifts

30   between each image. As SIM has developed, diverse strategies have been proposed for creation of the SIM

31   pattern [1,8–13]. Several different approaches for processing the data have also been introduced [3,7,8,14–16].

32   Recently, microscope systems capable of imaging with high resolution and a large field of view (FOV)

33   have been developed [17–21], some using custom-made microscope objectives. However, stitching together images

34   acquired with a higher magnification objective to create a large mosaic remains a valid and popular approach. Some

35   published results involving stitched images suffer from pronounced artifacts in which the edges of the individual

36   sub-images are visible, usually as dark bands which outline each sub-image [22–24]. On the other hand, several

37   studies have proposed methods for stitching of microscope images with reduced artifacts [25–32].

38   The combination of SIM with image stitching methods allows collection of large FOV images with both

39   optical sectioning and super-resolution properties. Here, we demonstrate methods and provide complete datasets for

40   five different samples. The samples are hematoxylin and eosin (H&E) stained histological specimens which provide

41   examples of human diseases (ovarian cancer, breast cancer, prostate cancer, skin cancer, and tuberculosis), and

42   which are also available commercially for those who wish to reproduce our work. We used freely available optical

43   designs [6,10,33] and open source software [33] for SIM imaging, along with freely available software for image

44   stitching (Microsoft Image Composite Editor (ICE) [34], or a well validated plugin [26] for ImageJ [35]).

45   Combining this with devignetting methods, we produced stitched images which are free of noticeable artifacts from

46   stitching or from SIM reconstruction.

47   Fluorescence microscopy is becoming more important in histopathology. Traditional bright field

48   microscopy diagnostic methods require a time-consuming process, involving chemical fixation and physical

49   sectioning. The use of optical sectioning fluorescence microscopy allows high-quality images to be captured without

50   the need for physical sectioning. Consequently, it has been shown that imaging can be performed on large human

51 tissue samples within 1 hour after excision [36]. Additionally, other studies have shown the results of fluorescence

52 imaging to be usable and accurate in diagnosis of various medical conditions [37–42]. Previously, it was noted that

53 obvious stitching artifacts significantly decrease the usability of large fluorescence images in medical diagnosis. In

54 one case, such artifacts resulted in the rejection of over half of the images acquired [38]. The setup we describe here

55 allows for fast, artifact-free, high-resolution imaging of fluorescent samples, and is compatible with samples stained

56 with most fluorescent dyes.

57 **Methods**

58 *Samples*

59   All samples used in this study are available from Carolina Biological, Omano, or Ward's Science. The

60 samples are approximately 7 μm thick and are stained with hematoxylin and eosin. The commercial source, product

61 number, and other SIM imaging parameters for each sample are detailed in Table 1. Table 2 details imaging

62 parameters for acquisitions of each sample with a color camera.

63 Table 1: Imaging parameters for the SIM datasets

Sample	Source company and product no.	SIM pattern no. of phases	Exposure time, ms	No. of tiles	Objective mag/NA	Acquisition time, s	Stitching software
Carcinoma of Prostate	Carolina, 318492	5	50	23 × 11	20×/0.45	315	Microsoft ICE
Basal Cell Carcinoma	Ward's Science, 470183-256	6	75	29 × 18	30×/1.05	821	FIJI
Adenocarcinoma of Ovary	Carolina, 318628	5	100	25 × 14	10×/0.4	595	Microsoft ICE
Adenocarcinoma of Breast	Carolina, 318766	8	200	12 × 8	10×/0.4	278	FIJI
Lung Tuberculosis	Omano, OMSK-HP50	5	100	20 × 16	30×/1.05	541	FIJI

64 Table 2: Parameters for the color images

Sample	No. of tiles	Objective mag/NA
Carcinoma of Prostate	6 × 5	4×/0.16
Basal Cell Carcinoma	5× 5	4×/0.16
Adenocarcinoma of Ovary	11 × 11	4×/0.16
Adenocarcinoma of Breast	6 × 6	4×/0.16
Lung Tuberculosis	8 × 10	10×/0.4

65 *Microscope setup and data acquisition*

66   We used a home-built SIM setup based on the same design as described previously [6,10,15] (Figure 1).

67 The SIM system is based on an IX83 microscope (Olympus) equipped with a Zyla 4.2+ sCMOS camera (Andor)

68 under the control of IQ3 software (Andor). We used the following Olympus objectives: UPLSAPO 4×/0.16 NA,

69   UPLSAPO 10×/0.4 NA, LUCPLFLN 20×/0.45 NA, and UPLSAPO 30×/1.05 NA silicone oil immersion. For color

70   images we used an aca1920-40uc color camera (Basler) under control of Pylon software (Basler). We used a MS-

71   2000 motorized microscope stage (Applied Scientific Instrumentation) to acquire tiled SIM images. In all datasets,

72   the stage scanning was configured such that all image edges overlapped by 20%.

73   Briefly, the SIM system uses a ferroelectric liquid crystal on silicon (LCOS) microdisplay (type SXGA-

74   3DM, Forth Dimension Displays). This device has been used previously in SIM and related methods in fluorescence

75   microscopy [5,10,15,33,43–47] and allows one to produce patterns of illumination on the sample which can be

76   reconfigured at will by changing the image displayed on the device. The light source (Lumencor Spectra-X) is

77   toggled off between SIM patterns and during camera readout. Figure 1 shows a simplified diagram of the

78   microscope system.

79   **INSERT FIGURE 1-system diagram**

80   *Motorized stage and illumination control*

81   Close synchronization between the camera acquisitions, light source, and microdisplay ensures rapid image

82   acquisition, helps reduce artifacts, and reduces light exposure to the sample. As shown in Figure 2, Andor IQ

83   software controls the SIM system.

84   **INSERT FIGURE 2-connection diagram**

85   While the camera and XYZ stage receive signals directly from Andor IQ software and an input/output computer

86   card (Measurement Computing DDA06/16), the illumination signals which the software generates must be altered

87   before being sent to the light source. Firstly, the microdisplay used in our setup will not produce an image on the

88   sample if it is illuminated with a constant light source. Rather, a meaningful illumination pattern will only form if

89   the light source is synchronized with an enable signal output from the microdisplay control board. Therefore, the

90   channel signals output by IQ are first modulated with the microdisplay enable signal (this is performed by the

91   leftmost AND gates pictured in Figure 2). Additionally, to reduce unnecessary light exposure to the sample, the light

92   source is shut off whenever the camera sensor is not being exposed. This is accomplished by performing a second

93   logical AND of the result of the previous AND with the 'FIRE' signal output from the camera. This process is

94   illustrated in Figure 3.

95   **INSERT FIGURE 3-trigger**

96   *SIM data processing*

97   SIM reconstructions were performed in the same way as previously described using SIMToolbox, an open-

98   source and freely available program that our group developed for processing SIM data [33]. We generated optically

99   sectioned, enhanced resolution images using a Bayesian estimation method, maximum *a posteriori* probability SIM

100   (MAP-SIM) [15]. MAP-SIM works using maximum *a posteriori* probability methods, which are well known in

101   microscopy applications [48,49], to enhance high spatial frequency image information. We then combine this

102   information, in the frequency domain, with low spatial frequency image information obtained by OS-SIM methods,

103   then produce the final image by an inverse Fourier transform [15]. We typically measure the final resolution

104   obtained by analyzing the frequency spectrum of the resulting image, as is discussed below.

105   The illumination patterns used here are generated such that the sum of all positions in each pattern set

106   results in homogenous illumination. As such, a widefield (WF) image can be reconstructed from SIM data simply by

107   performing an average intensity projection of the patterned images. This can be described by

$$I_{WF} = \frac{1}{N} \sum_{n=1}^{N} I_n,$$

108

109   where N is the number of pattern phases, I_n is the image acquired on the nth illumination position, and I_{WF} is the WF

110   reconstruction. This is the method we used to generate WF images throughout this study.

111   *Vignetting correction*

112   Following SIM reconstruction, vignetting artifacts remain in each tile. If not removed prior to stitching, this

113   vignetting introduces a distracting grid pattern in the final stitched image. We performed vignette removal by

114   dividing each tile of the mosaic by an image representing the vignetting profile common to all tiles. Other studies

115   have used an image of a uniformly fluorescent calibration slide as a reference for vignette removal [36], where

116   information concerning non-uniform illumination is captured. However, we found that SIM processing introduces

117   vignetting artifacts beyond those due to non-uniform illumination. Additionally, these artifacts vary somewhat

118   depending on properties of the sample being imaged. As such, performing pre-acquisition calibration on a uniformly

119   fluorescent slide is not sufficient to remove vignetting artifacts from SIM reconstructions. Instead, an estimate of the

120   vignetting profile is found through analysis of the mosaic tiles after SIM reconstruction.

121   A blurred average intensity projection of the tiles is a good approximation of the vignetting profile, as an

122   average intensity projection merges the tiles into a single image with averaged foreground information while

123   preserving the vignetting profile. Subsequent blurring with an appropriate radius and edge-handling method also

124   eliminates the high spatial frequency foreground without impacting the low spatial frequency illumination profile.

125   To eliminate errors during the blurring step due to the blurring area extending outside the original image, we used an

126   edge handling method in which the blurring area is reduced near the edges of the image such that no values outside

127   the image border are sampled. Unlike edge handling methods in which the image is padded with a uniform value (or

128   mirrored and tiled) to accommodate a blurring area which extends beyond the original image limits, this method is

129   free from major artifacts, such as erroneous brightness of the image edges, see figure 4. While the average intensity

130   projection removes most foreground information from the images, some coarseness remains in the vignette

131   estimation after this step (figure 4a), especially for stitches with fewer than 50 tiles. The blurring step serves to

132   eliminate only this non-vignette information and must preserve the illumination profile. As shown in figure 4b, use

133   of the default Gaussian blurring function in ImageJ introduces a bright glow near to borders of the image, a

134   significant artifact which does not reflect the original vignetting profile. Use of the 'border limited mean' filter, on

135   the other hand, does not introduce this aberration, as shown in figure 4c.

136   **INSERT FIGURE 4-edge method**

137   Approximating the illumination profile works especially well for histological samples, as such samples are

138   non-sparse and require many tiles, factors which improve the accuracy of this approach. We performed all steps of

139   this devignetting process using built-in functions and the 'Fast Filters' plugin in ImageJ [50]. The effect of

140   devignetting is illustrated in Figure 5.

141   **INSERT FIGURE 5-devignetting**

142   *Image Stitching*

143   With visible vignetting removed, we then stitched together a composite image from the tiles. The pre-

144   processing allows for stitching to be done in various stitching applications; Microsoft ICE and Preibisch's plugin for

145   FIJI [26] were used to stitch the data presented here.

146   The data processing procedure described here is summarized in Figure 6. The total time for processing each

147   dataset was about 30 min.

148   **INSERT FIGURE 6-flowchart**

149   *Color image data processing methods*

150   We created color overview images by stitching devignetted brightfield acquisitions. Devignetting was

151   performed simply by adding the inverse of an empty brightfield acquisition to each color tile using ImageJ. For this

152   method to produce optimal results, the empty brightfield image must be acquired in conditions identical to those of

153   the raw tile data, such that the illumination profile in the empty image matches that of the unprocessed tiles. This

154   simple operation removes nearly all visible vignetting and color balance artifacts within each tile. The results after

155   devignetting were then stitched using Preibisch's plugin for FIJI [26].

156   *Resolution measurement*

157   We evaluated our results by measuring image resolution using SR Measure Toolbox. SR Measure

158   Toolbox [51] measures the resolution limit of input images through analysis of the normalized, radially averaged

159   power spectral density (PSD_{ca}) of the images, as previously described [6]. Briefly, the resolution limit in real space

160   is determined by evaluating the cutoff frequency in Fourier space. The cutoff frequency is estimated by calculating

161   the spatial frequency at which the PSD_{ca} (after noise correction) drops to zero.

162   Focusing on the basal cell carcinoma sample, we selected 125 (out of 522 total) image tiles, calculated the

163   PSD and resolution for each tile, and averaged the results. We found that, in the case of this sample, the image

164   resolution was 593 ± 20 nm for WF and 468 ± 2.5 nm for MAP-SIM (average ± standard deviation). This data was

165   acquired with a UPLSAPO 30×/1.05 NA silicone oil immersion objective. Figure 7 shows an example measurement

166   for one image tile. Figure 8 shows a plot of PSD_{ca} for this image tile.

167   **INSERT FIGURE 7-resolution**

168   **INSERT FIGURE 8-PSD**

169   **Results**

170   Figure 9 shows images of a prepared slide containing a human prostate carcinoma sample stained with

171   H&E. Figure 9a shows a stitched color overview, and Figure 9d shows a zoom-in of the region indicated in Figure

172   9a, acquired separately using a UPLSAPO 20×/0.75NA objective. Figure 9b shows a stitched widefield fluorescence

173   image, and Figure 9c shows a stitched SIM image. Figures 9e and 9f each show zoom-ins of the stitches shown in

174   Figures 9b and 9c, respectively. Using the acquisition and processing methods described, whole-slide images are

175   produced without any visible stitching artifacts. Additionally, the MAP-SIM reconstruction method produces

176   resolution superior to that of the widefield data. Figures 10-13 show similar comparisons for basal cell carcinoma,

177   ovary adenocarcinoma, breast adenocarcinoma, and tuberculosis of the lung, respectively.

178   The data shown in figures 9-13 is freely available through Giga DB[52]. This dataset includes all color

179   overviews as well as WF and MAP-SIM stitches at full resolution. In addition, all image tiles used to create the WF

180   and MAP-SIM stitches of the samples are provided.

181   **INSERT FIGURE 9-prostate**

182   **INSERT FIGURE 10-basal cell**

183   **INSERT FIGURE 11-ovary**

184   **INSERT FIGURE 12-breast**

185   **INSERT FIGURE 13-lung**

186   **Discussion**

187   Many past studies into stitching of SIM mosaics have suffered from noticeable image artifacts, arising from

188   flaws in the optical setups used as well as imperfections in the SIM reconstruction and image stitching processes.

189   While these artifacts are sometimes minimal enough to remain uncorrected, certain artifacts seriously inhibit the

190   usefulness of the final stitched image. In [23], the authors note that issues in triggering and evenly illuminating the

191   microdisplay being used for illumination resulted in striping and vignetting artifacts; similarly, in [22,24,36,53],

192   stitching artifacts are apparent in the images.

193   Here, optimization of the optical setup, camera-microdisplay synchronization, and image processing

194   methods yielded whole-slide images free from visible SIM or image stitching artifacts. In addition to the elimination

195   of artifacts, our use of SIMToolbox to perform SIM reconstruction on the data allows for a variety of reconstruction

196   algorithms to be used, including super-resolution algorithms such as MAP-SIM. This too presents an improvement

197   over previous works.

198   Another advantage of the acquisition and processing methods demonstrated here is the minimization of

199   user intervention, and in turn, reductions in acquisition and processing time. Stage movement, sample focusing,

200   image acquisition, and SIM pattern advancement are controlled automatically. Loading of the sample, definition of

201   the mosaic edges, and manual focus on 3-5 positions in the sample are the only steps needed to be taken by the user

202   before acquisition can begin. Recent developments in autofocus technology for SIM may allow for the manual focus

203   step to be shortened or omitted [53]. These automated steps during acquisition allow for large mosaics to be

204   acquired. The quality of the final stitched images does not degrade for larger mosaics – in fact, the quality of the

205   devignetting process improves with larger datasets, as more data is available to produce an accurate estimation of

206   the illumination profile. SIMToolbox (version 2.0), which is capable of utilizing the processing power of modern

207   consumer graphics cards during MAP-SIM processing, also reduces the time spent during the data processing phase.

208   Finally, unlike other super-resolution reconstruction methods such as SR-SIM, MAP-SIM is able to produce artifact-

209   free results without tuning of reconstruction parameters by the user, a process which is difficult to automate and

210   requires significant user experience.

211   One drawback of the method presented here is the inability to image the entire volume of samples thicker

212   than ~0.5 mm. However, this limitation does not prevent large, unsectioned samples from being imaged, as is the

213   case with bright field microscopy, where samples must be thin enough for transmitted light to reach the objective.

214   Rather, as the light which illuminates the sample in fluorescence microscopy emanates from the objective, all

215   surface regions of a large sample may be imaged. Additionally, due to the optical sectioning exhibited by SIM, light

216   from out-of-focus regions of the sample is almost completely attenuated. Consequently, imaging the surfaces of

217   large samples with SIM produces high quality images without the need for physical sectioning, as previously

218   demonstrated [23,36].

219   Here, we demonstrated our imaging techniques on traditionally prepared histopathological samples in order

220   to provide a comparison between bright field imaging and SIM, but the same techniques can be used to image a

221   wide variety of fluorescently labelled samples. The ability to seamlessly image the entire surface region of large

222   samples has multiple potential applications in histopathology. SIM presents unique advantages in analyzing the

223   surgical margins of large tissue excisions, as demonstrated by Wang, et al [36]. Confocal imaging of core needle

224   biopsy samples has been previously demonstrated to produce images suitable for medical diagnosis [42], a practice

225   easily adapted to SIM. The speed at which sample preparation and image acquisition can be performed in

226   fluorescence microscopy presents opportunities for intra-operative analysis of tissue samples using SIM techniques,

227   as mentioned by multiple other studies [23,36,54,55].

228   **Reuse potential and example of data reuse**

229   The data provided here presents various opportunities for reuse. With the multiple high-resolution color

230   overviews and stitched SIM images, comparison of structures visible in the brightfield and fluorescent images could

231   be performed to further study the use of fluorescence microscopy in histopathology. The unstitched image tiles of

232   the basal cell carcinoma sample provided in the dataset, which still contain vignetting artifacts, may be used to

233   reproduce the results of our devignetting process, as well as to further develop new devignetting approaches suited

234   for SIM. These tiles might also be used to create or modify existing stitching software for global minimization of

235   stitching artifacts. Note that the image tiles from the other samples in the dataset are provided after devignetting.

236   Gone uncorrected, vignetting in the image tiles used to stitch a larger image can cause a noticeable grid

237   pattern in the final stitched image. While readily noticeable upon viewing of the image, quantification of this pattern

238   is useful for evaluation of methods which remove it. Since this stitching artifact arises from an illumination profile

239   common to each tile, the period of this pattern in the stitched image can simply be represented by the spacing

240   between tiles used during acquisition:

241
$$T_{stitch} = l \cdot (1 - r),$$

242   where l is the image width and r is the proportional overlap between image tiles. The parameters for the dataset

243   visualized in Figure 14 are $l = 2048$ px and $r = 0.2$, thus $T_{stitch} = 1638$ px, or ~355 μm (as the dataset has a pixel size

244   of ~216.7 nm). In our setup, the camera sensor is square, so T_{stitch} is the same both the horizontally and vertically in

245   the final image. As a pattern with a very consistent period, this grid artifact manifests in the FFT of an uncorrected

246   stitch as series of bright peaks. As shown in Fig 14e, the location of the peaks corresponding to the fundamental

247   frequency of the grid pattern agrees very well with the calculated T_{stitch}. Figs. 14d and 14e show that the FFT of a

248   properly corrected image contains no trace of the peaks evident in the uncorrected image.

249   **INSERT FIGURE 14-analysis**

250   **Availability of source code and requirements**

251   Project name: SIMToolbox version 2.12

252   Project home page: http://mmtg.fel.cvut.cz/SIMToolbox/

253   Operating system: platform independent

254   Programming language: MATLAB

255   License: GNU General Public License v3.0

256   **Detailed software compatibility notes**

257   The SIMToolbox GUI was compiled with MATLAB 2015a and tested in Windows 7 and 8. The GUI is a stand-alone

258   program and does not require MATLAB to be installed. To use the MATLAB functions within SIMToolbox (i.e.,

259   without the GUI), MATLAB must be installed. The functions were mainly developed with 64 bit MATLAB versions

260   2012b, 2014a, 2015a in Windows 7. When using SIMToolbox functions without the GUI, the MATLAB "Image

261   Processing Toolbox" is required. SIMToolbox also requires the "MATLAB YAML" package to convert MATLAB

262   objects to/from YAML file format. Note that this package is installed automatically when using the GUI.

263   **Availability of data**

264   All raw and analyzed data is available on GigaDB [52]. All files and data are distributed under the Creative Commons

265   CC0 waiver, with a request for attribution. The data is organized into five main folders for the five different samples,

266   see table 3.

267   Table 3: Description of the data files

Folder	Files	File Size
01-Prostate-carcinoma	Prostate-carcinoma-WF-tiles.zip	3.6 GB
	Prostate-carcinoma-MAPSIM-tiles.zip	3.5 GB
	Prostate-carcinoma-WF-stitch.tif	695 Mb
	Prostate-carcinoma-MAPSIM-stitch.tif	695 Mb
	Prostate-carcinoma-Color-stitch.tif	118 MB
02-Basal-cell-carcinoma	Basal-cell-carcinoma-MAPSIM-tiles.zip	7.5 GB

	Basal-cell-carcinoma-WF-tiles.zip	7.5 GB
	Basal-cell-carcinoma-MAPSIM-stitch.tif	6.3 GB
	Basal-cell-carcinoma-WF-stitch.tif	5.7 GB
	Basal-cell-carcinoma-color-stitch.tif	123 MB
03-Ovary-adenocarcinoma	Ovary-adenocarcinoma-MAPSIM-tiles.zip	891 MB
	Ovary-adenocarcinoma-WF-tiles.zip	849 MB
	Ovary-adenocarcinoma-MAPSIM-stitch.tif	916 MB
	Ovary-adenocarcinoma-WF-stitch.tif	979 MB
	Ovary-adenocarcinoma-Color-stitch.tif	610 MB
04-Breast-adenocarcinoma	Breast-adenocarcinoma-MAPSIM-tiles.zip	1.4 GB
	Breast-adenocarcinoma-WF-tiles.zip	1.4 GB
	Breast-adenocarcinoma-MAPSIM-stitch.tif	1.1 GB
	Breast-adenocarcinoma-WF-stitch.tif	1.1 GB
	Breast-adenocarcinoma-Color-stitch.tif	129 MB
05-Lung-tuberculosis	Lung-tuberculosis-MAPSIM-tiles.zip	4.8 GB
	Lung-tuberculosis-WF-tiles.zip	4.6 GB
	Lung-tuberculosis-MAPSIM-stitch.tif	3.8 GB
	Lung-tuberculosis-WF-stitch.tif	3.6 GB
	Lung-tuberculosis-Color-stitch.tif	341 MB

268

Abbreviations

Av Int Proj, average intensity projection; FOV, field of view; H&E, hematoxylin and eosin; ICE, Image Composite

Editor; MAP-SIM, maximum *a posteriori* probability SIM; NA, numerical aperture; LCOS, liquid crystal on silicon;

PSDca, circularly averaged power spectral density; SIM, structured illumination microscopy; WF, wide field.

Ethics approval and consent to participate

Because the samples were acquired commercially, and because they are completely de-identified (meaning that there

is no way to connect these particular samples to the original donor), this is not considered human subject research,

and approval is not required to work with these samples.

Consent for publication

Not applicable

Competing interests

The authors declare that they have no competing interests.

Author Contributions

KJ: acquired data, analyzed data, wrote the paper

GH: conceived project, acquired data, analyzed data, supervised research, wrote the paper

References

1. M. A. A. Neil, R. Juškaitis, and T. Wilson, "Method of obtaining optical sectioning by using structured light in a conventional microscope," Opt. Lett. **22**, 1905–1907 (1997).

2. M. G. L. Gustafsson, "Surpassing the lateral resolution limit by a factor of two using structured illumination microscopy," J. Microsc. **198**, 82–87 (2000).

3. R. Heintzmann and C. Cremer, "Laterally modulated excitation microscopy: improvement of resolution by using a diffraction grating," Proc. SPIE **3568**, 185–196 (1998).

4. L. Schermelleh, P. M. Carlton, S. Haase, L. Shao, L. Winoto, P. Kner, B. Burke, M. C. Cardoso, D. A. Agard, M. G. L. Gustafsson, H. Leonhardt, and J. W. Sedat, "Subdiffraction multicolor imaging of the nuclear periphery with 3D structured illumination microscopy," Science **320**, 1332–1336 (2008).

5. R. Fiolka, L. Shao, E. H. Rego, M. W. Davidson, and M. G. L. Gustafsson, "Time-lapse two-color 3D imaging of live cells with doubled resolution using structured illumination," Proc. Natl. Acad. Sci. U. S. A. **109**, 5311–5315 (2012).

6. J. Pospíšil, T. Lukeš, J. Bendesky, K. Fliegel, K. Spendier, and G. M. Hagen, "Imaging tissues and cells beyond the diffraction limit with structured illumination microscopy and Bayesian image reconstruction," Gigascience **8**, giy126 (2019).

7. X. Huang, J. Fan, L. Li, H. Liu, R. Wu, Y. Wu, L. Wei, H. Mao, A. Lal, P. Xi, L. Tang, Y. Zhang, Y. Liu, S.

309   Tan, and L. Chen, "Fast, long-term, super-resolution imaging with Hessian structured illumination

310   microscopy," Nat. Biotechnol. **36**, 451–459 (2018).

311   8.   M. G. L. Gustafsson, L. Shao, P. M. Carlton, C. J. R. Wang, I. N. Golubovskaya, W. Z. Cande, D. A. Agard,

312   and J. W. Sedat, "Three-dimensional resolution doubling in widefield fluorescence microscopy by structured

313   illumination," Biophys. J. **94**, 4957–4970 (2008).

314   9.   S. Rossberger, G. Best, D. Baddeley, R. Heintzmann, U. Birk, S. Dithmar, and C. Cremer, "Combination of

315   structured illumination and single molecule localization microscopy in one setup," J. Opt. **15**, 094003

316   (2013).

317 10.   P. Křížek, I. Raška, and G. M. Hagen, "Flexible structured illumination microscope with a programmable

318   illumination array," Opt. Express **20**, 24585 (2012).

319 11.   P. Kner, B. B. Chhun, E. R. Griffis, L. Winoto, and M. G. L. Gustafsson, "Super-resolution video

320   microscopy of live cells by structured illumination," Nat. Methods **6**, 339–342 (2009).

321 12.   L. J. Young, F. Ströhl, and C. F. Kaminski, "A Guide to Structured Illumination TIRF Microscopy at High

322   Speed with Multiple Colors," J. Vis. Exp. e53988–e53988 (2016).

323 13.   V. Poher, H. X. Zhang, G. T. Kennedy, C. Griffin, S. Oddos, E. Gu, D. S. Elson, M. Girkin, P. M. W.

324   French, M. D. Dawson, and M. A. Neil, "Optical sectioning microscope with no moving parts using a micro-

325   stripe array light emitting diode," Opt. Express **15**, 11196–11206 (2007).

326 14.   F. Orieux, E. Sepulveda, V. Loriette, B. Dubertret, and J.-C. Olivo-Marin, "Bayesian estimation for

327   optimized structured illumination microscopy.," IEEE Trans. Image Process. **21**, 601–14 (2012).

328 15.   T. Lukeš, P. Křížek, Z. Švindrych, J. Benda, M. Ovesný, K. Fliegel, M. Klíma, and G. M. Hagen, "Three-

329   dimensional super-resolution structured illumination microscopy with maximum a posteriori probability

330   image estimation," Opt. Express **22**, 29805–17 (2014).

331 16.   T. Lukeš, G. M. Hagen, P. Křížek, Z. Švindrych, K. Fliegel, and M. Klíma, "Comparison of image

332   reconstruction methods for structured illumination microscopy," Proc. SPIE **9129**, 91293J (2014).

333 17.   C. A. Werley, M.-P. Chien, and A. E. Cohen, "An ultrawidefield microscope for high-speed fluorescence

334   imaging and targeted optogenetic stimulation," Biomed. Opt. Express **8**, 5794 (2017).

335 18.   N. J. Sofroniew, D. Flickinger, J. King, and K. Svoboda, "A large field of view two-photon mesoscope with

336   subcellular resolution for in vivo imaging," Elife **5**, (2016).

337   19.   G. McConnell, J. Trägårdh, R. Amor, J. Dempster, E. Reid, and W. B. Amos, "A novel optical microscope

338   for imaging large embryos and tissue volumes with sub-cellular resolution throughout," Elife **5**, (2016).

339   20.   P. J. Keller, A. D. Schmidt, J. Wittbrodt, and E. H. K. Stelzer, "Reconstruction of zebrafish early embryonic

340   development by scanned light sheet microscopy," Science **322**, 1065–1069 (2008).

341   21.   J. N. Stirman, I. T. Smith, M. W. Kudenov, and S. L. Smith, "Wide field-of-view, multi-region, two-photon

342   imaging of neuronal activity in the mammalian brain," Nat. Biotechnol. **34**, 857–862 (2016).

343   22.   B. Migliori, M. S. Datta, C. Dupre, M. C. Apak, S. Asano, R. Gao, E. S. Boyden, O. Hermanson, R. Yuste,

344   and R. Tomer, "Light sheet theta microscopy for rapid high-resolution imaging of large biological samples,"

345   BMC Biol. **16**, 57 (2018).

346   23.   T. C. Schlichenmeyer, M. Wang, K. N. Elfer, and J. Q. Brown, "Video-rate structured illumination

347   microscopy for high-throughput imaging of large tissue areas," Biomed. Opt. Express **5**, 366 (2014).

348   24.   D. Xu, T. Jiang, A. Li, B. Hu, Z. Feng, H. Gong, S. Zeng, and Q. Luo, "Fast optical sectioning obtained by

349   structured illumination microscopy using a digital mirror device," J. Biomed. Opt. **18**, 060503 (2013).

350   25.   F. B. Legesse, O. Chernavskaia, S. Heuke, T. Bocklitz, T. Meyer, J. Popp, and R. Heintzmann, "Seamless

351   stitching of tile scan microscope images," J. Microsc. **258**, 223–232 (2015).

352   26.   S. Preibisch, S. Saalfeld, and P. Tomancak, "Globally optimal stitching of tiled 3D microscopic image

353   acquisitions," Bioinformatics **25**, 1463–1465 (2009).

354   27.   C. Murtin, C. Frindel, D. Rousseau, and K. Ito, "Image processing for precise three-dimensional registration

355   and stitching of thick high-resolution laser-scanning microscopy image stacks," Comput. Biol. Med. **92**, 22–

356   41 (2018).

357   28.   J. Chalfoun, M. Majurski, T. Blattner, K. Bhadriraju, W. Keyrouz, P. Bajcsy, and M. Brady, "MIST:

358   Accurate and Scalable Microscopy Image Stitching Tool with Stage Modeling and Error Minimization," Sci.

359   Rep. **7**, 4988 (2017).

360   29.   Y. Yu and H. Peng, "Automated high speed stitching of large 3D microscopic images," in *2011 IEEE*

361   *International Symposium on Biomedical Imaging: From Nano to Macro* (IEEE, 2011), pp. 238–241.

362   30.   A. Bria and G. Iannello, "TeraStitcher - A tool for fast automatic 3D-stitching of teravoxel-sized microscopy

363   images," BMC Bioinformatics **13**, 316 (2012).

364   31.   F. Yang, Z.-S. Deng, and Q.-H. Fan, "A method for fast automated microscope image stitching," Micron **48**,

365   17–25 (2013).

366   32.   P. Thévenaz and M. Unser, "User-friendly semiautomated assembly of accurate image mosaics in

367   microscopy," Microsc. Res. Tech. **70**, 135–146 (2007).

368   33.   P. Křížek, T. Lukeš, M. Ovesný, K. Fliegel, and G. M. Hagen, "SIMToolbox: A MATLAB toolbox for

369   structured illumination fluorescence microscopy," Bioinformatics **32**, 318–320 (2015).

370   34.   Microsoft, "Image Composite Editor," .

371   35.   C. A. Schneider, W. S. Rasband, and K. W. Eliceiri, "NIH Image to ImageJ: 25 years of image analysis,"

372   Nat. Methods **9**, 671–675 (2012).

373   36.   M. Wang, D. B. Tulman, A. B. Sholl, H. Z. Kimbrell, S. H. Mandava, K. N. Elfer, S. Luethy, M. M.

374   Maddox, W. Lai, B. R. Lee, and J. Q. Brown, "Gigapixel surface imaging of radical prostatectomy

375   specimens for comprehensive detection of cancer-positive surgical margins using structured illumination

376   microscopy," Sci. Rep. **6**, 27419 (2016).

377   37.   J. L. Dobbs, H. Ding, A. P. Benveniste, H. M. Kuerer, S. Krishnamurthy, W. Yang, and R. Richards-

378   Kortum, "Feasibility of confocal fluorescence microscopy for real-time evaluation of neoplasia in fresh

379   human breast tissue," J. Biomed. Opt. **18**, 106016 (2013).

380   38.   D. S. Gareau, "Feasibility of digitally stained multimodal confocal mosaics to simulate histopathology," J.

381   Biomed. Opt. **14**, 034050 (2009).

382   39.   M. T. Tilli, M. C. Cabrera, A. R. Parrish, K. M. Torre, M. K. Sidawy, A. L. Gallagher, E. Makariou, S. A.

383   Polin, M. C. Liu, and P. A. Furth, "Real-time imaging and characterization of human breast tissue by

384   reflectance confocal microscopy," J. Biomed. Opt. **12**, 051901 (2007).

385   40.   A. Parrish, E. Halama, M. T. Tilli, M. Freedman, and P. A. Furth, "Reflectance confocal microscopy for

386   characterization of mammary ductal structures and development of neoplasia in genetically engineered

387   mouse models of breast cancer," J. Biomed. Opt. **10**, 051602 (2005).

388   41.   Y. Chen, W. Xie, A. K. Glaser, N. P. Reder, C. Mao, S. M. Dintzis, J. C. Vaughan, and J. T. C. Liu, "Rapid

389   pathology of lumpectomy margins with open-top light-sheet (OTLS) microscopy," Biomed. Opt. Express

390   **10**, 1257 (2019).

391   42.   J. Dobbs, S. Krishnamurthy, M. Kyrish, A. P. Benveniste, W. Yang, and R. Richards-Kortum, "Confocal

392   fluorescence microscopy for rapid evaluation of invasive tumor cellularity of inflammatory breast carcinoma

393   core needle biopsies," Breast Cancer Res. Treat. **149**, 303–310 (2015).

394   43.   G. M. Hagen, W. Caarls, K. A. Lidke, A. H. B. De Vries, C. Fritsch, B. G. Barisas, D. J. Arndt-Jovin, and T.

395   M. Jovin, "Fluorescence recovery after photobleaching and photoconversion in multiple arbitrary regions of

396   interest using a programmable array microscope," Microsc. Res. Tech. **72**, 431–440 (2009).

397   44.   S. R. Kantelhardt, W. Caarls, A. H. B. de Vries, G. M. Hagen, T. M. Jovin, W. Schulz-Schaeffer, V. Rohde,

398   A. Giese, and D. J. Arndt-Jovin, "Specific visualization of glioma cells in living low-grade tumor tissue,"

399   PLoS One **5**, 1–11 (2010).

400   45.   L. Shao, P. Kner, E. H. Rego, and M. G. L. Gustafsson, "Super-resolution 3D microscopy of live whole cells

401   using structured illumination," Nat. Methods **8**, 1044–1046 (2011).

402   46.   B.-C. Chen, W. R. Legant, K. Wang, L. Shao, D. E. Milkie, M. W. Davidson, C. Janetopoulos, X. S. Wu, J.

403   A. Hammer, Z. Liu, B. P. English, Y. Mimori-Kiyosue, D. P. Romero, A. T. Ritter, J. Lippincott-Schwartz,

404   L. Fritz-Laylin, R. D. Mullins, D. M. Mitchell, J. N. Bembenek, A.-C. Reymann, R. Bohme, S. W. Grill, J.

405   T. Wang, G. Seydoux, U. S. Tulu, D. P. Kiehart, and E. Betzig, "Lattice light-sheet microscopy: Imaging

406   molecules to embryos at high spatiotemporal resolution," Science **346**, 1257998 (2014).

407   47.   G. M. Hagen, W. Caarls, M. Thomas, A. Hill, K. A. Lidke, B. Rieger, C. Fritsch, B. van Geest, T. M. Jovin,

408   and D. J. Arndt-Jovin, "Biological applications of an LCoS-based programmable array microscope," Proc.

409   SPIE **64410S**, 1–12 (2007).

410   48.   H. Hurwitz, "Entropy reduction in Bayesian analysis of measurements," Phys. Rev. A **12**, 698–706 (1975).

411   49.   P. J. Verveer and T. M. Jovin, *Efficient Superresolution Restoration Algorithms Using Maximum a*

412   *Posteriori Estimations with Application to Fluorescence Microscopy* (1997), Vol. 14, p. 1696.

413   50.   Michael Schmid, "Fast Filters," . https://imagej.nih.gov/ij/plugins/download/misc/Fast_Filters.java

414   51.   J. Pospíšil, K. Fliegel, and M. Klíma, "Assessing resolution in live cell structured illumination microscopy,"

415   in *Proceedings of SPIE - The International Society for Optical Engineering*, P. Páta and K. Fliegel, eds.

416   (SPIE, 2017), Vol. 10603, p. 39.

417   52.   Johnson KA; Hagen GM (2020): Supporting data for "Artifact-free whole-slide imaging with structured

418   illumination microscopy and Bayesian image reconstruction" GigaScience Database.

419   http://dx.doi.org/10.5524/100728

420   53   T. C. Schlichenmeyer, M. Wang, C. Wenk, J. Q. Brown, and J. Q. Brown, "Autofocus optimization for

421   tracking tissue surface topography in large-area mosaicking structured illumination microscopy," in

422   *Frontiers in Optics 2014* (OSA, 2014), p. FM4F.3.

423   54.   H. L. Fu, J. L. Mueller, M. P. Javid, J. K. Mito, D. G. Kirsch, N. Ramanujam, and J. Q. Brown,

424   "Optimization of a Widefield Structured Illumination Microscope for Non-Destructive Assessment and

425   Quantification of Nuclear Features in Tumor Margins of a Primary Mouse Model of Sarcoma," PLoS One **8**,

426   e68868 (2013).

427   55.   H. L. Fu, J. L. Mueller, M. J. Whitley, D. M. Cardona, R. M. Willett, D. G. Kirsch, J. Q. Brown, and N.

428   Ramanujam, "Structured Illumination Microscopy and a Quantitative Image Analysis for the Detection of

429   Positive Margins in a Pre-Clinical Genetically Engineered Mouse Model of Sarcoma," PLoS One **11**,

430   e0147006 (2016).

431

FIGURE CAPTIONS

433   Figure 1: Simplified diagram of SIM system. LCOS, liquid crystal on silicon

434   Figure 2. Simplified connection diagram.

435   Figure 3. Illumination trigger signal logic. This logical operation occurs for each illumination wavelength at the

436   rightmost AND gates pictured in Figure 2.

437   Figure 4: Edge handling during the blurring process. (a) is the result after performing an average intensity projection

438   on a set of MAP-SIM tiles. (b) shows (a) after being blurred using ImageJ's 'Gaussian blur' with a radius of 200

439   pixels, while (c) shows (a) blurred using the 'border limited mean' filter.

440   Figure 5: Vignetting artifacts and their removal. (a) shows the result of stitching images without applying the

441   devignetting process, while (b) shows a stitch of the same data after devignetting has been applied. (c) shows the

442   average intensity projection of the images used to stitch (a), which estimates the vignette profile of each frame. This

443   estimate can be refined by application of an edge-limited blurring filter, as shown in (d). (e) shows the average

444   intensity projection of the data used in (b), after devignetting has been applied. The uniform brightness of (e)

445   indicates that no major vignetting artifacts remain in the devignetted data.

446   Figure 6. Panoramic SIM data processing workflow. Devignetting was performed after SIM reconstruction. Note the

447   vignette profile differs between reconstruction methods, necessitating separate projection, blurring and division

448   steps. Av Int Proj, average intensity projection.

449   Figure 7. Evaluating image resolution. (a) and (b) show a tile from the data in Figure 10 (basal cell carcinoma

450   sample) after widefield and MAP-SIM reconstruction, respectively. (c) and (d) each show a zoom-in of (a) and (b),

451   respectively. (e) and (f) each show the FFT of (a) and (b), respectively. The dotted lines in (e) and (f) indicate the

452   resolution of each image according to the resolution measurement described.

453   Figure 8. Normalized, radially averaged power spectral density (PSD_{ca}) and resolution analysis measured on the tiles

454   shown in Figs. 7a and 7b.

455   Figure 9: Carcinoma of human prostate. (a) Color overview, (b) WF stitch, (c) MAP-SIM stich. (d) shows a region

456   of the sample indicated in (a). (e) and (f) each show a zoom-in of (b) and (c), respectively, in the region indicated in

457   (a).

458   Figure 10: Basal Cell Carcinoma. (a) Color overview, (b) WF stitch, (c) MAP-SIM stich. (d) shows a region of the

459   sample indicated in (a). (e) and (f) each show a zoom-in of (b) and (c), respectively, in the region indicated in (a).

460   Figure 11: Adenocarcinoma of human ovary. (a) Color overview, (b) WF stitch, (c) MAP-SIM stich. (d), (g) show a

461   region of the sample indicated in (a), acquired separately from (a) using a 10× objective. (e) and (h) show a zoom-in

462   of (b), while (f) and (i) show a zoom-in of (c), all in the regions indicated in (a).
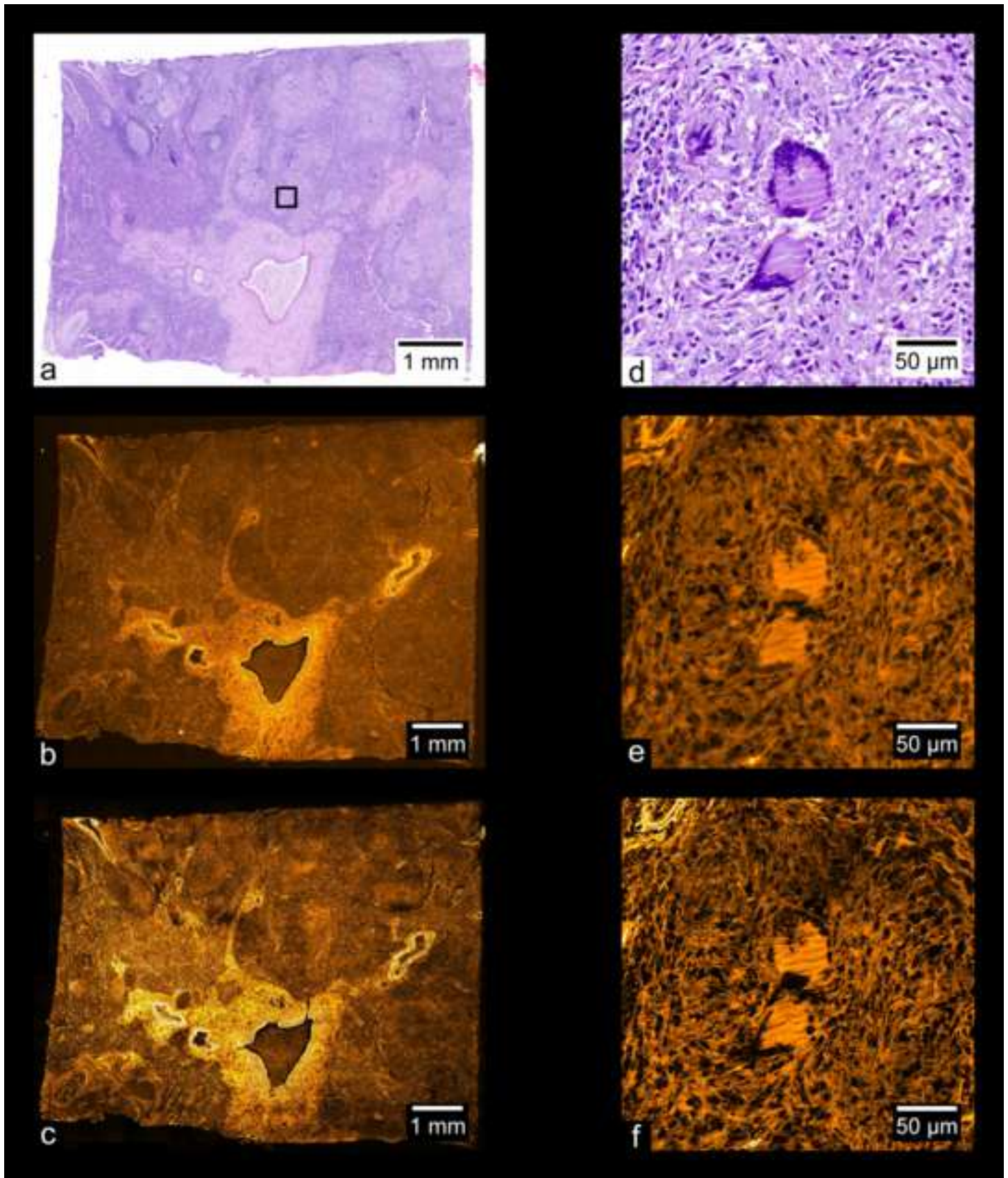
463   Figure 12: Adenocarcinoma of human breast. (a) Color overview, (b) WF stitch, (c) MAP-SIM stich. (d) shows a

464   region of the sample indicated in (a), acquired separately from (a) using a 10× objective. (e) and (f) each show a

465   zoom-in of (b) and (c), respectively, in the region indicated in (a).
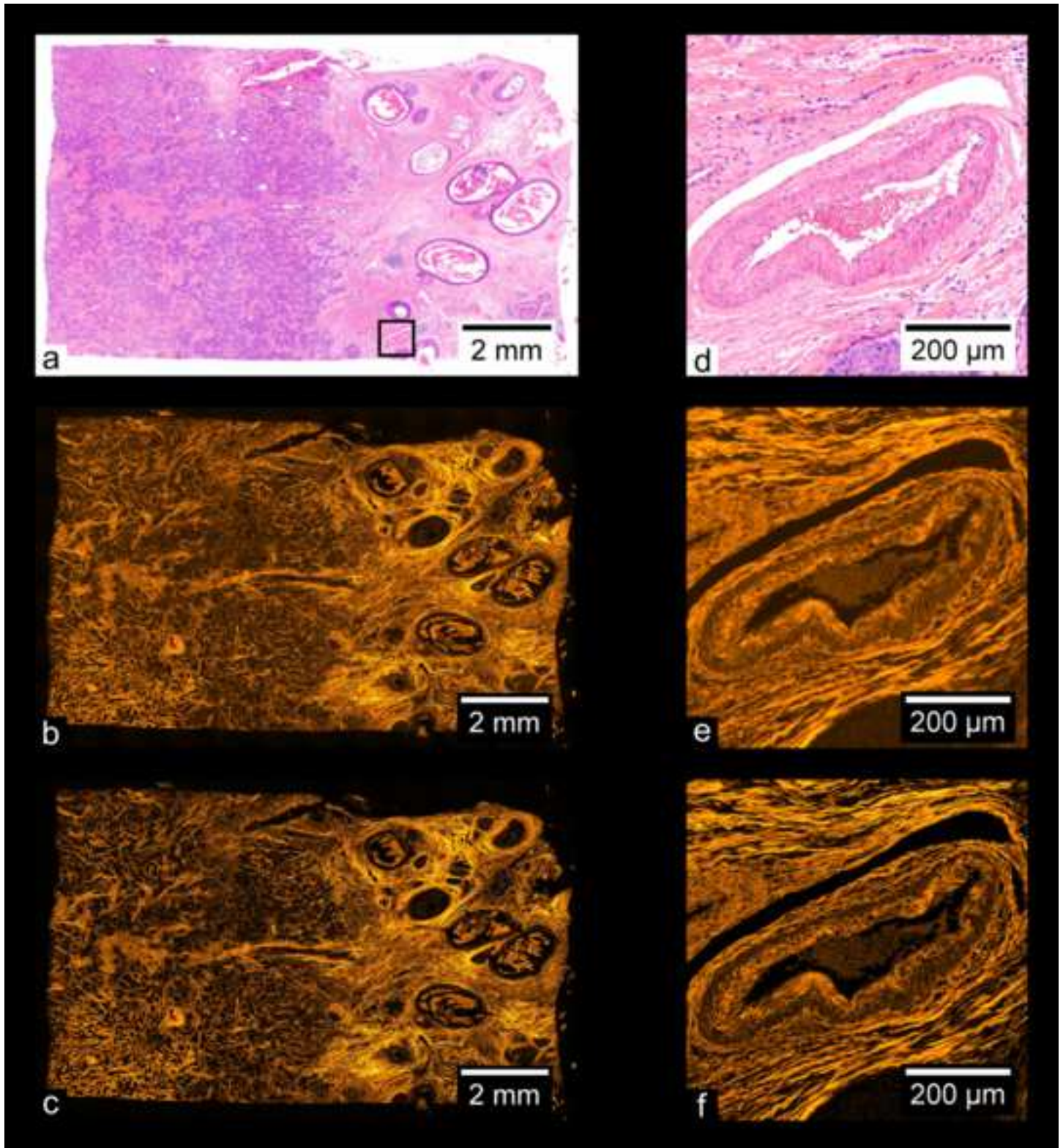
466   Figure 13: Tuberculosis of human lung. (a) Color overview, (b) WF stitch, (c) MAP-SIM stich. (d) shows a region

467   of the sample indicated in (a), acquired separately from (a) using a 20× objective. (e) and (f) each show a zoom-in of

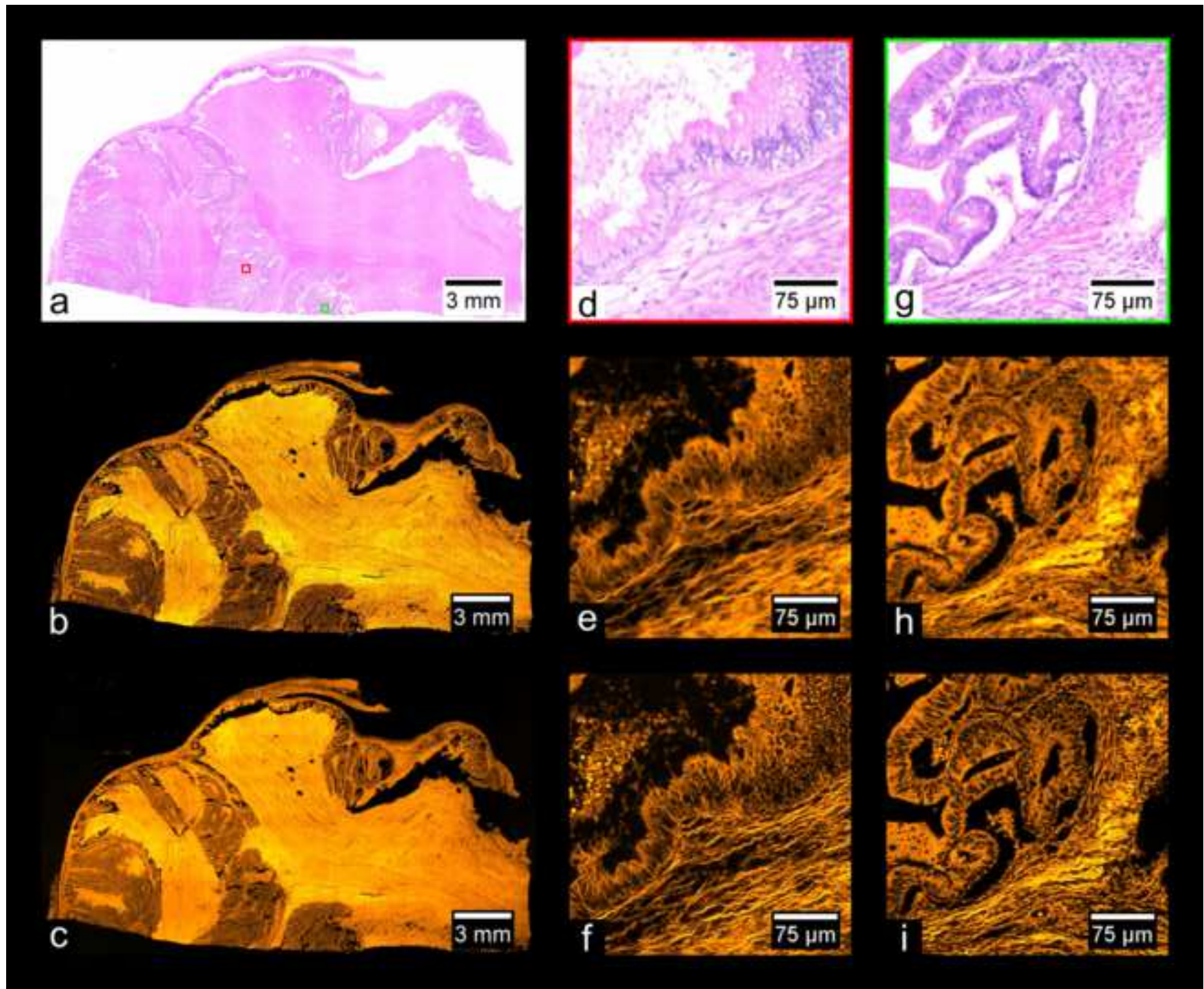468   (b) and (c), respectively, in the region indicated in (a).

469   Figure 14: Analysis of periodic stitching artifacts in the frequency domain. (a) shows a stitched image where

470   devignetting has not been applied to the tiles, while (b) shows a stitch of devignetted data. (c) and (d) show the
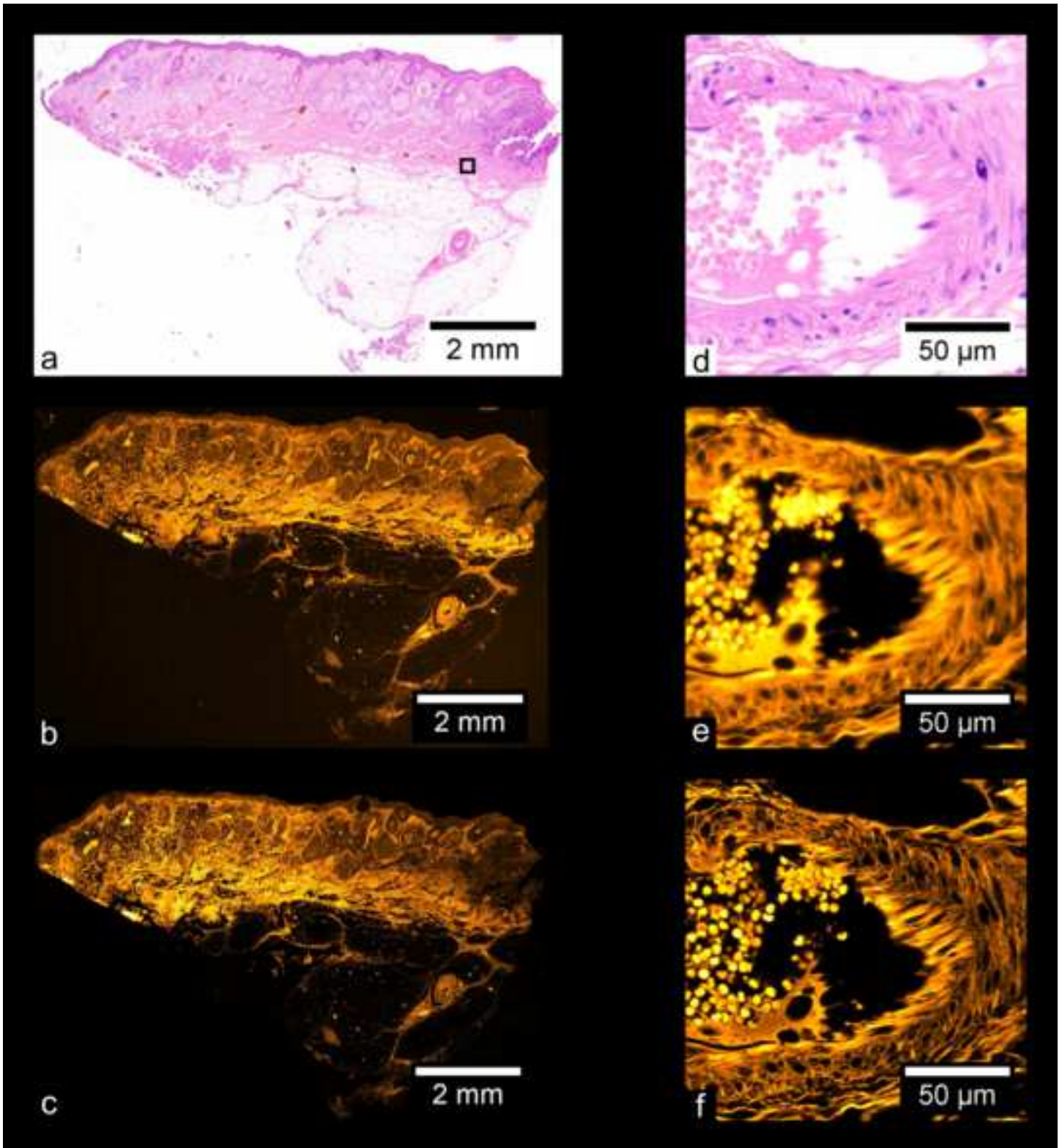
471   central region of the FFT's of (a) and (c), respectively. The arrows in (c) point to the fundamental peaks of the grid

472   artifact. (e) shows plots of (c) and (d) through the center of each image along the x and y axes. The calculated value

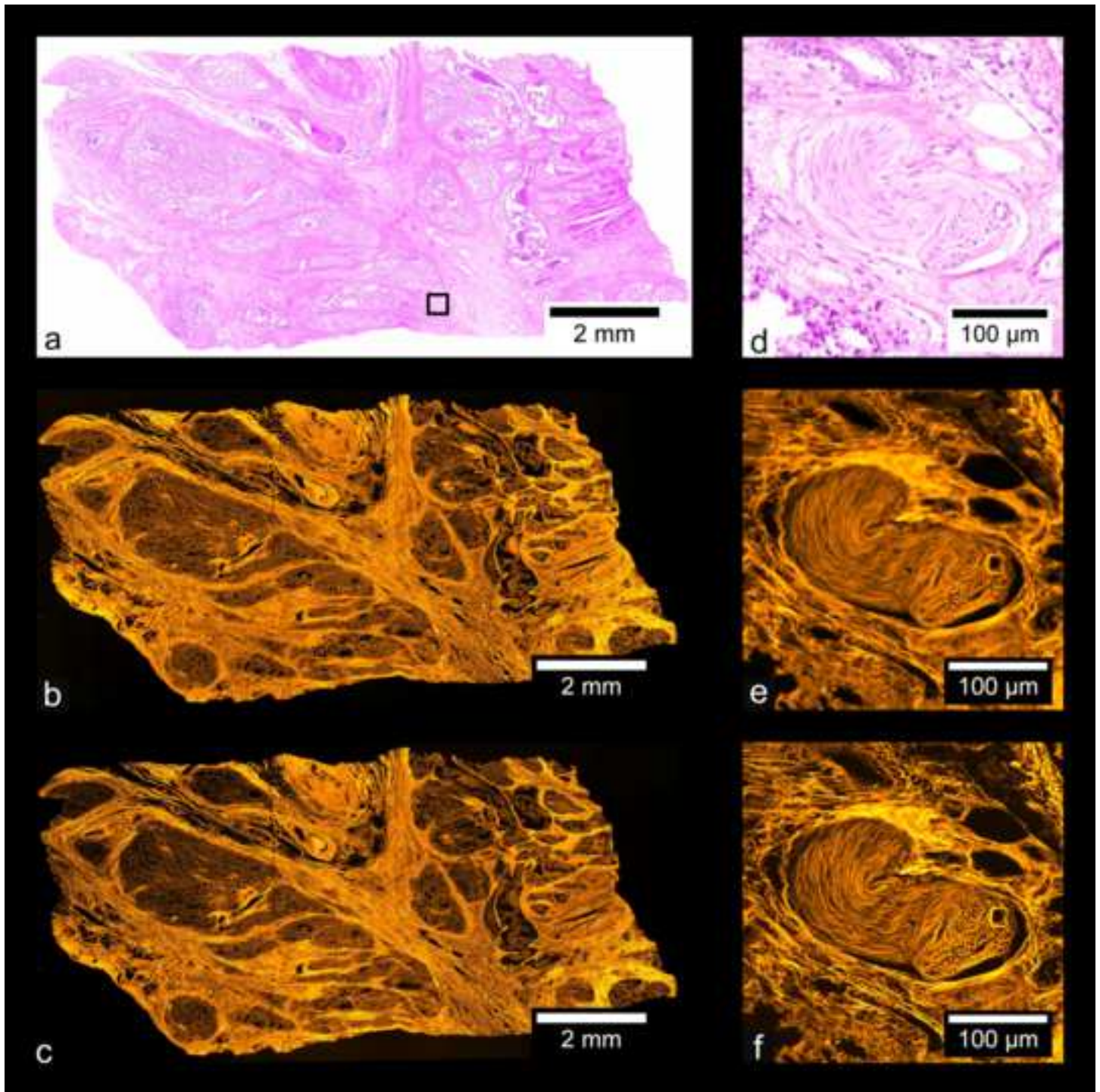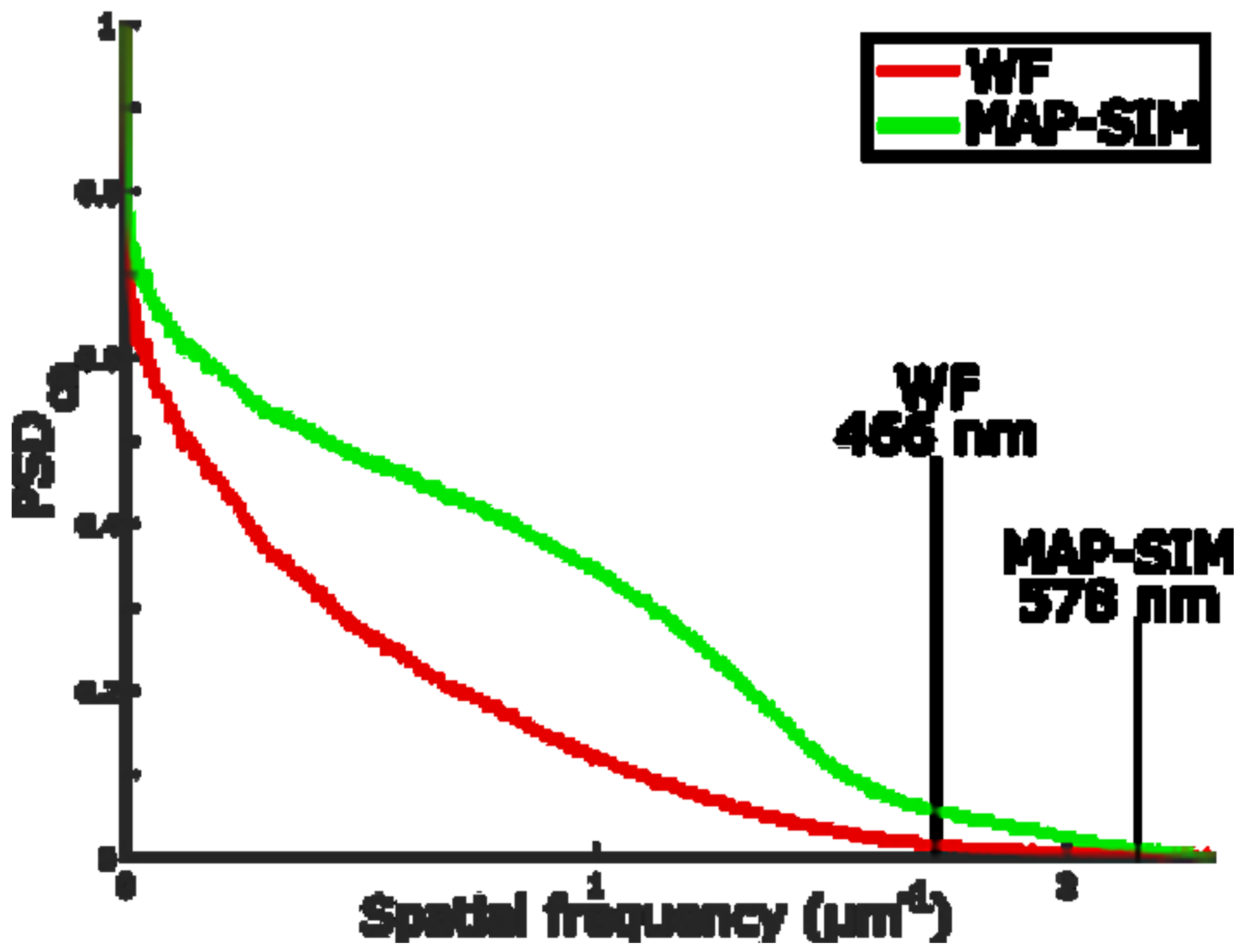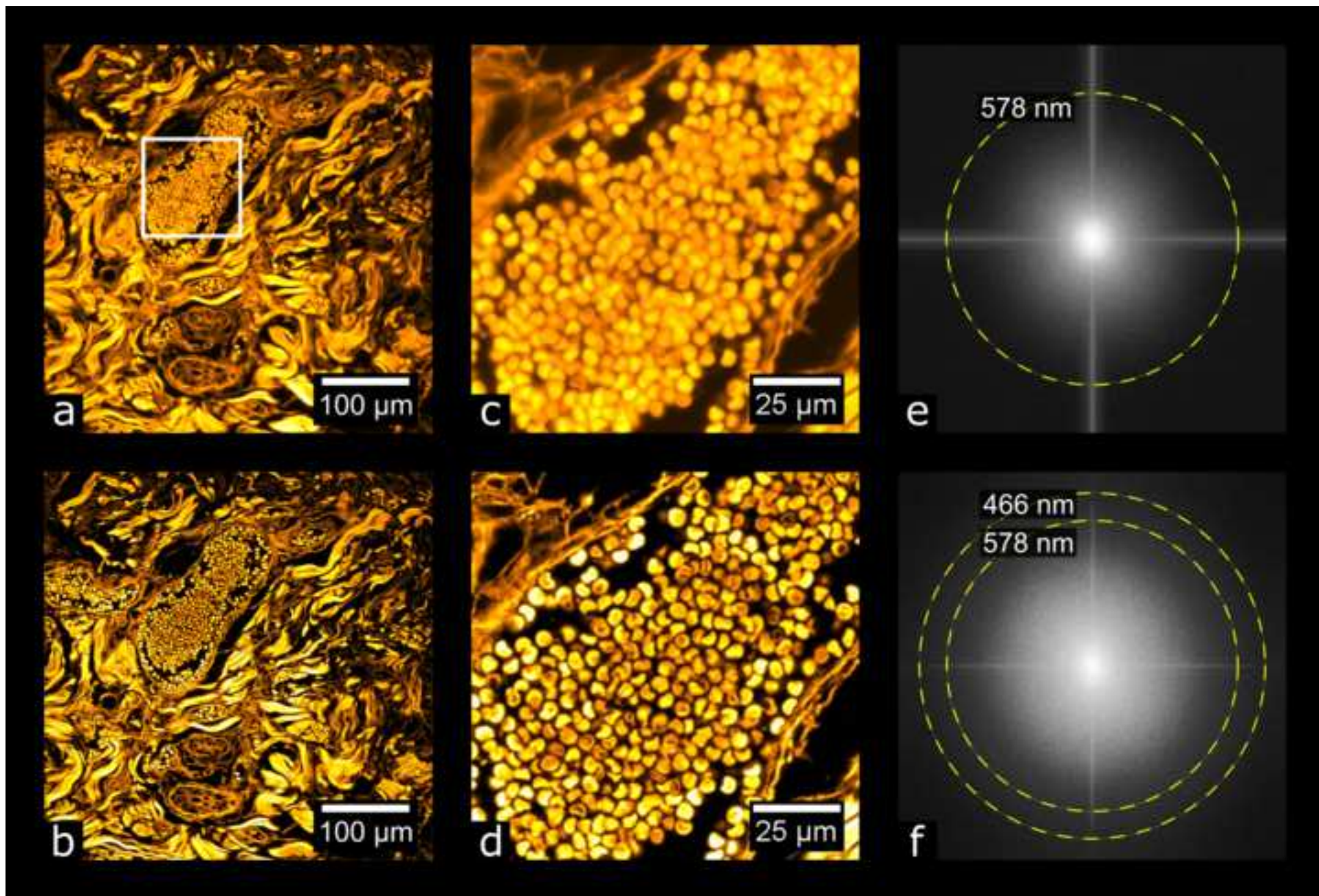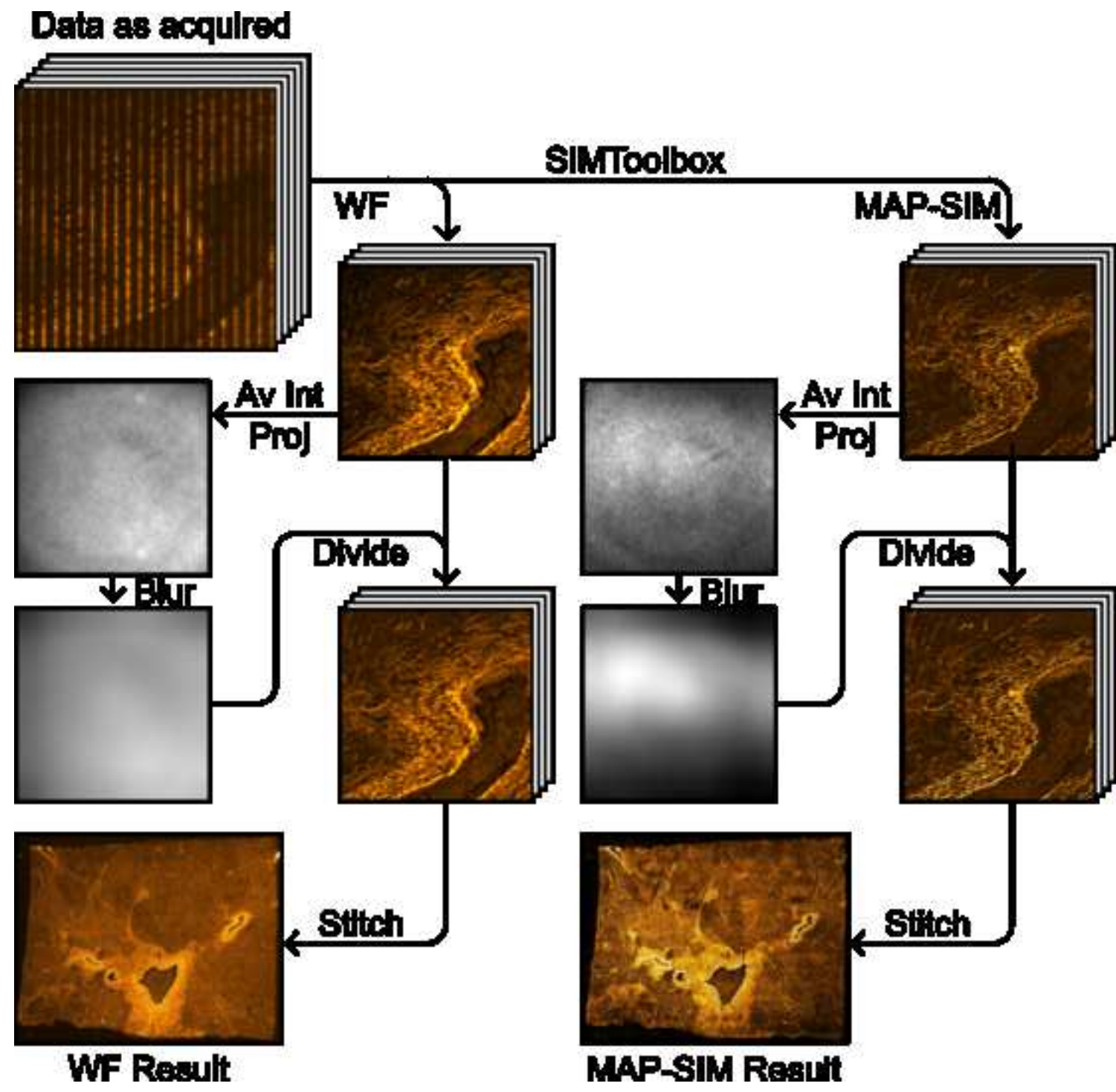473   for T_{stitch} aligns very well with the peaks along both axes.

Figure11-ovary

Figure10-basal cell

Figure09-prostate

Figure08-PSD

Figure07-resolution

Figure05-devignetting

Figure04-edge method

Figure03-trigger

Figure02-connection diagram
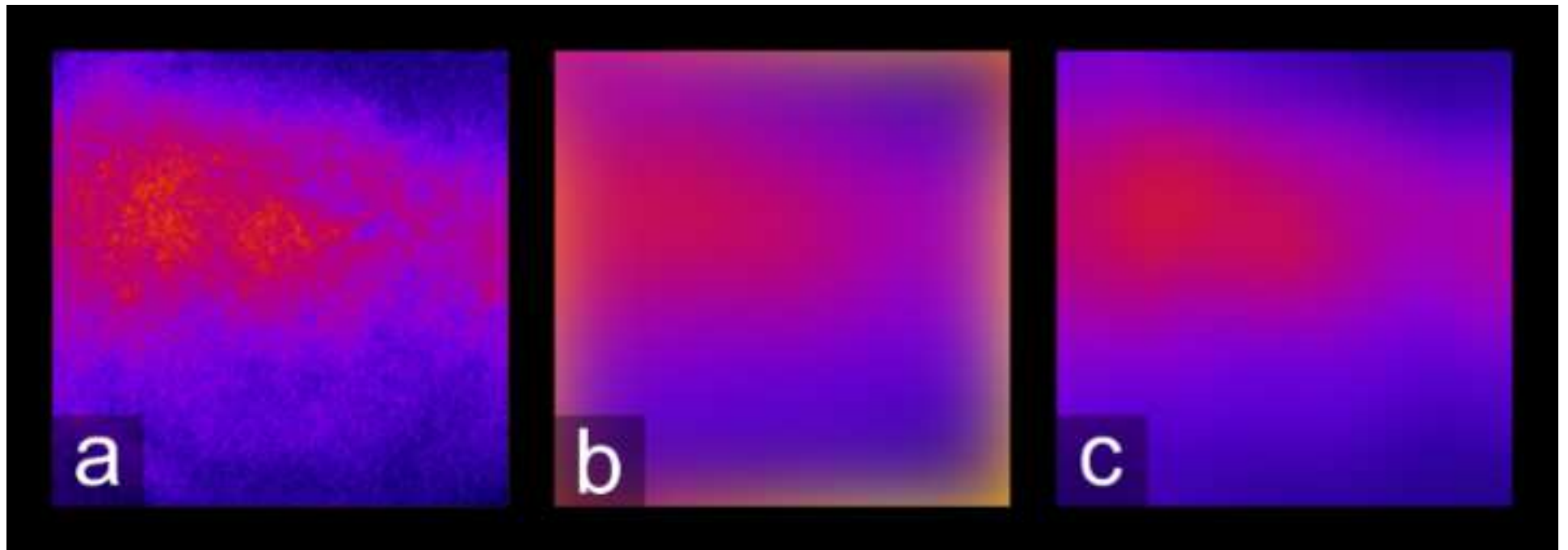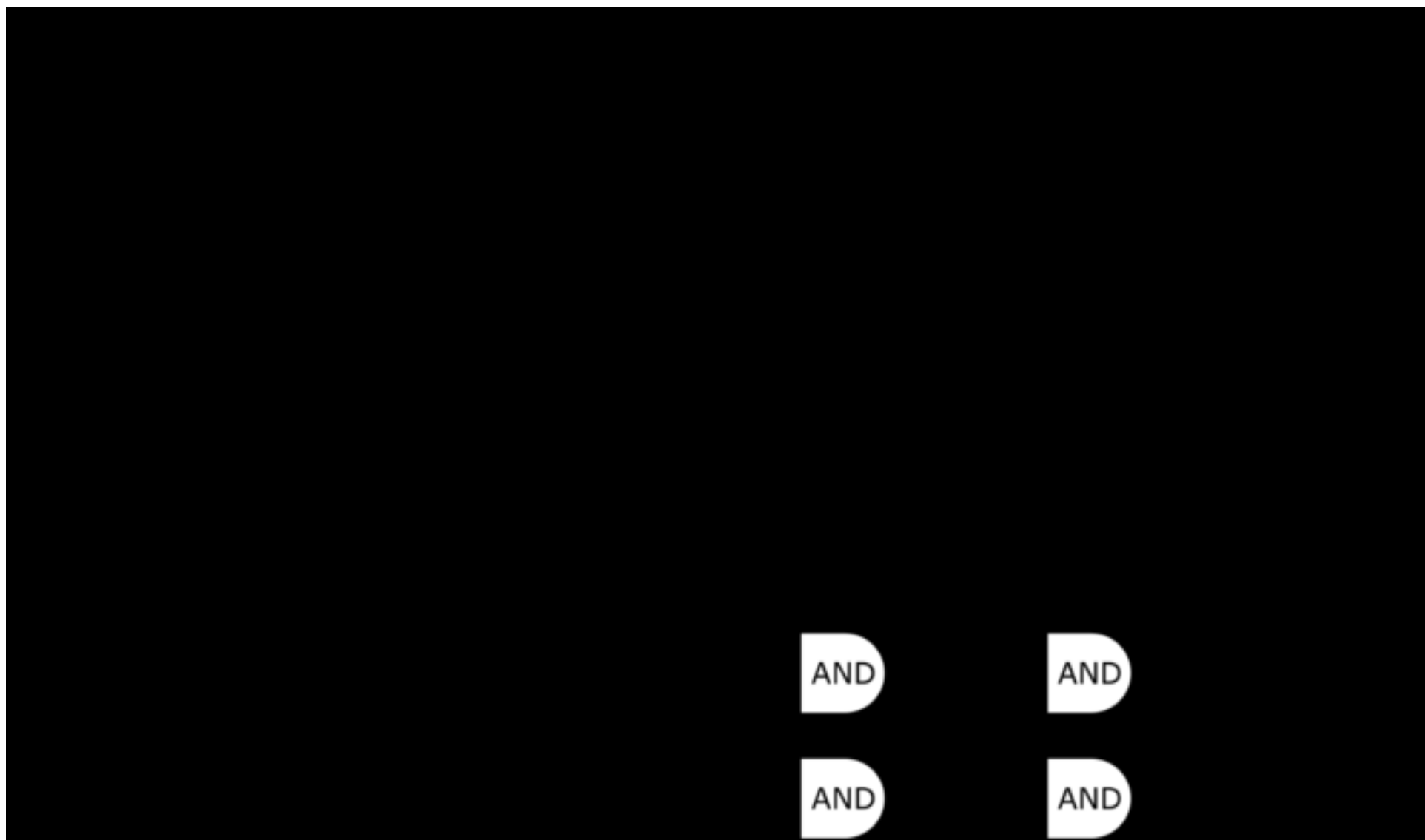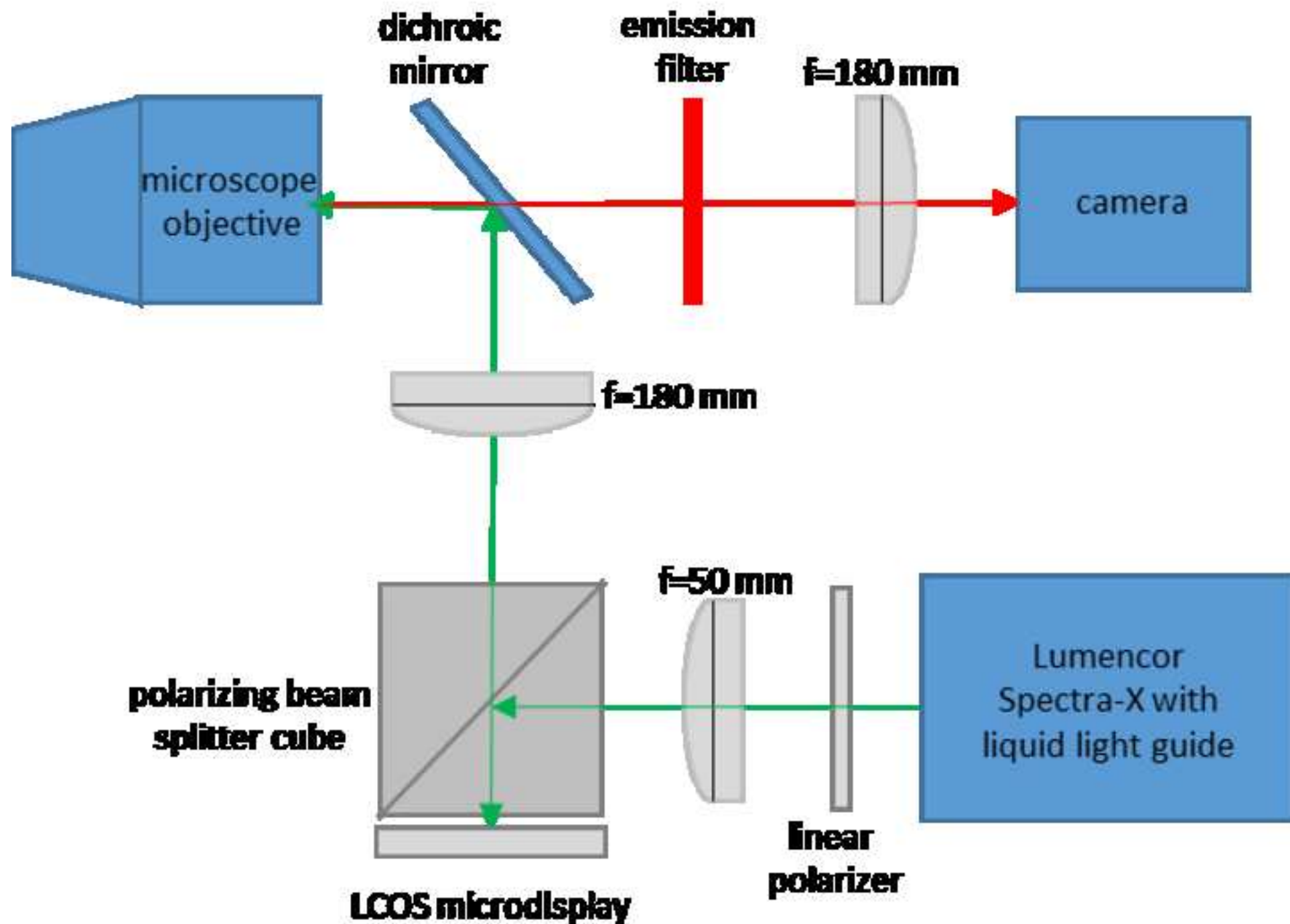
Figure01-system diagram
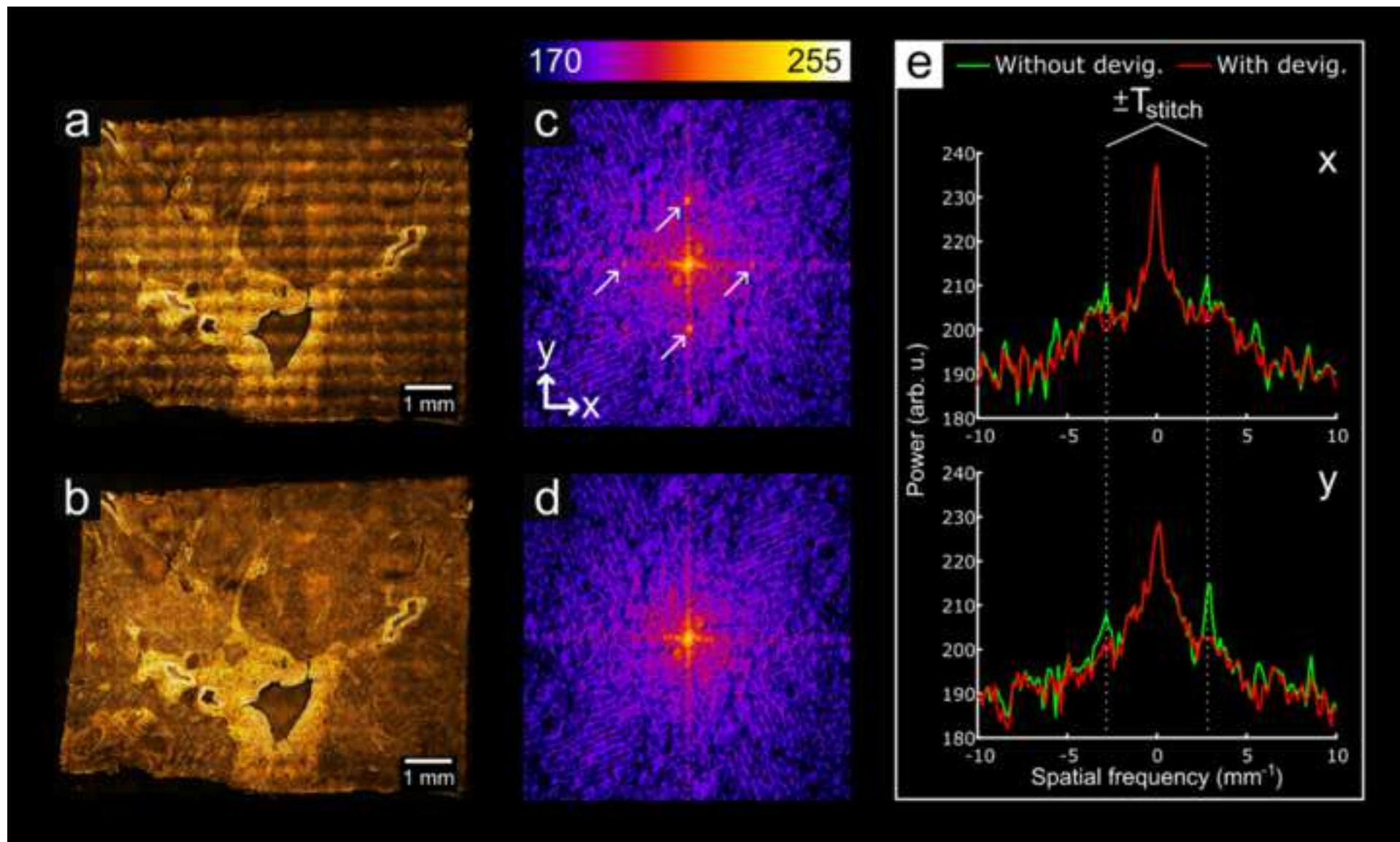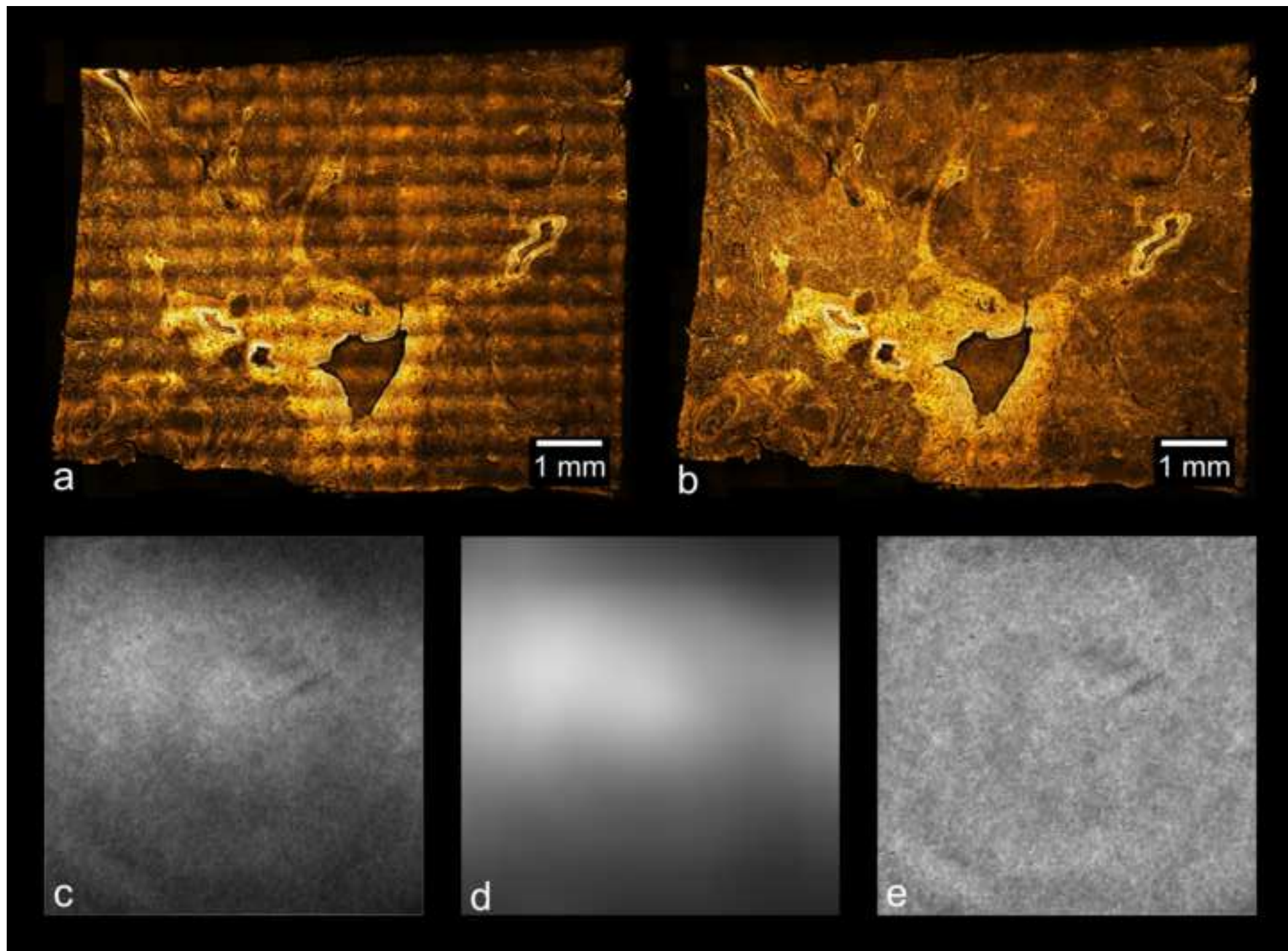
University of Colorado Colorado Springs

UCCS

Dr. Guy M. Hagen

Biofrontiers

1420 Austin Bluffs Pkwy.

Colorado Springs, CO 80918

Tel. 719-255-3692

ghagen@uccs.edu

Dear Editor:

We would like to re-submit our manuscript entitled "Artifact-free whole-slide imaging with structured illumination microscopy and Bayesian image reconstruction" for consideration in *GigaScience* as a data note. We made the following revisions.

1. The reviewer noticed that two of the data files was incomplete or corrupted. We reloaded these two files.

2. We included a table showing the organization of the data files along with their sizes.

3. We included a universal public domain dedication text file with the dataset.

4. We added a statement about ethics approval and consent to participate.

5. We moved all of the information from the supplement into the main paper. We removed the example of the cellular-scale imaging.

We hope that our paper will now be acceptable for publication in GigaScience.

Sincerely,

Guy M. Hagen